Lab on a Chip

PAPER

View Article Online
View Journal | View Issue

Cite this: *Lab Chip*, 2016, **16**, 1861

Motorized actuation system to perform droplet operations on printed plastic sheets†

Taejoon Kong,‡ Riley Brien,‡ Zach Njus, Upender Kalwa and Santosh Pandey*

We developed an open microfluidic system to dispense and manipulate discrete droplets on planar plastic sheets. Here, a superhydrophobic material is spray-coated on commercially-available plastic sheets followed by the printing of hydrophilic symbols using an inkjet printer. The patterned plastic sheets are taped to a two-axis tilting platform, powered by stepper motors, that provides mechanical agitation for droplet transport. We demonstrate the following droplet operations: transport of droplets of different sizes, parallel transport of multiple droplets, merging and mixing of multiple droplets, dispensing of smaller droplets from a large droplet or a fluid reservoir, and one-directional transport of droplets. As a proof-of-concept, a colorimetric assay is implemented to measure the glucose concentration in sheep serum. Compared to silicon-based digital microfluidic devices, we believe that the presented system is appealing for various biological experiments because of the ease of altering design layouts of hydrophilic symbols, relatively faster turnaround time in printing plastic sheets, larger area to accommodate more tests, and lower operational costs by using off-the-shelf products.

Received 5th February 2016,
Accepted 7th April 2016

DOI: 10.1039/c6lc00176a

www.rsc.org/loc

Introduction

Generally speaking, microfluidic platforms consist of closed-channel networks where liquid flow is controlled by mechanical, pneumatic or electrokinetic means. Today, with emphasis on higher experimental throughput, microfluidic platforms incorporate several on-chip components (*e.g.* microvalves, micropumps, and microelectrodes) that increase the complexity in fabricating the different layers, integrating the micro- and macroscale components, and controlling the individual sensing or actuation parts.[1,2] In contrast to closed-channel microfluidics, open microfluidic platforms obviate the use of polymeric channels and continuous liquid flow; thereby relaxing the fabrication process, easing the system integration to fewer components, and promising a cheaper alternative to robotic micro-handling systems.[3,4] In open microfluidics, liquid is dispensed from a reservoir as discretized droplets and transported to desired locations for further manipulation. Typical operations to be performed with discrete droplets may include transport of a single or multiple droplets, merging and mixing of two droplets, incubation and affinity binding within droplets, extraction of solid particles from the liquid phase, and removal of waste droplets.[3,5] These droplet operations are often conceptualized from test tube experiments performed in a wet chemistry laboratory, and the sequence of operations can be easily altered depending on the actual experiment being performed.

The general strategy of producing and actuating discrete droplets on open surfaces relies on methods to modulate the surface tension between the liquid droplet and the solid surface it rests on. The current literature on this topic can be grouped into two categories – methods that employ electrical fields to modulate the wettability of droplets[3–6] and non-electrical methods that employ mechanical, magnetic, acoustic or gravitational forces to generate directional movement of droplets.[7–15]

The electrical or 'electrowetting-on-dielectric' method of droplet actuation has gained popularity in the last decade primarily because of the ease of programmability and portability.[16,17] Here, the conductive liquid droplet sits on patterned electrodes coated with a hydrophobic dielectric layer. An electric field applied to the target electrode increases the contact angle of the droplet placed over it, and thus alters the wettability of the liquid surface to the solid surface. This electrowetting phenomenon can be scaled up to move and control multiple droplets over an array of electrodes, thereby performing any desired sequence of operations including transport, merging, mixing, splitting, and dispensing. Analogous to digital microelectronics where pockets of electrons are transferred between devices (*e.g.* in charged coupled devices), several groups have realized electrowetting-based 'digital microfluidic platforms' having electrodes of precisely-

Department of Electrical and Computer Engineering, Iowa State University, 1050 Coover Hall, Ames, IA 50011, USA. E-mail: pandey@iastate.edu

† Electronic supplementary information (ESI) available: Supplementary figures and videos of droplet manipulation included. See DOI: 10.1039/c6lc00176a

‡ Joint first authors.

controlled geometry, on-chip control electronics to energize individual electrodes, and software programs to automate the droplet operations.[3,18,19]

Even though the electrowetting method is widely accepted as the gold standard for droplet handling systems, it is restrained by the need for high electrical voltages (in the range of 100 volts to 400 volts) that have unknown effects on the biomolecules or cells within droplets.[18–20] For instance, the electric actuation force can interfere with the adsorption of biomolecules on a surface.[21] Furthermore, droplet actuation is dependent on the conductivity of the droplet and the dielectric properties of the insulating layers (*e.g.* Teflon and Parylene) that are expensive for large-scale deposition. Because each electrode is electrically addressed, there are only a finite number of electrodes that can be addressed on a digital microfluidics platform.[22] To get around this last issue, it has been shown that the electrodes can be optically stimulated (and thereby producing on-demand optical interconnects) by incorporating photoconductive and high dielectric constant layers underneath the Teflon coating.[8,23] Active matrix arrays of thin film transistor (TFTs) have also been demonstrated as an alternate digital microfluidic testbed where many thousand individually addressable electrodes could sense, monitor, and manipulate droplets.[22] Similarly, electrodes can be selectively energized to reposition water volumes in an otherwise liquid paraffin medium to create reconfigurable, continuous-flow microfluidic channels.[24] As these innovations in digital microfluidics technology extend the functionalities to newer arenas of portable diagnostics, much of the fabrication protocol still requires access of industrial-grade microelectronics foundry and is thus limited to select users.

To eliminate some of the limitations of electrowetting mentioned above, non-electrical methods of droplet actuation have been pursued.[9,11–15] In the 'textured ratchet' method, movement of liquid droplets is achieved on textured microstructures (*i.e.* ratchets) fabricated in silicon or elastomeric substrates.[15] The textured ratchets are placed on a level stage that is vertically vibrated using a linear motor. At the resonant frequency of vertical oscillations, the liquid droplet is able to advance or recede on the textured ratchets. The movement of different droplets can be individually controlled, both in linear and closed tracks, by manipulating the volume and viscosity of droplets. In the 'superhydrophobic tracks' method, shallow grooves are cut in zinc plates or silicon substrates.[14] This is followed by a superhydrophobic coating step by depositing silver and fluorinated thiol surfactant on metal plates or a fluoropolymer on silicon substrates. The produced superhydrophobic tracks are able to confine liquid droplets and guide their movement in trajectories defined by the tracks. In the 'surface acoustic waves (SAW)' method, a high frequency source connected to interdigitated gold electrodes generates acoustic waves that is able to transport fluid droplets on a piezoelectric substrate.[25] Recently, pneumatic suction through a PDMS membrane has been used to activate and move droplets in two dimensions on a superhydrophobic surface without any interference from an external energy (*e.g.* heat, light, electricity).[21]

While the above non-electrical methods demonstrate that mechanical machining the substrate can passively move droplets, more results are needed to match the level of droplet handling operations achieved in digital microfluidic platforms.[3] To gauge the maturity of digital microfluidics, an exciting example is a multi-functional digital microfluidic cartridge by Advanced Liquid Logic that can perform multiplexed real-time PCR, immunoassays and sample preparation.[26] A group at Sandia National Laboratories has developed a digital microfluidic distribution hub for next generation sequencing that is capable of executing sample preparation protocols and quantitative capillary electrophoresis for size-based quality control of the DNA library.[27] With growing demand of lab on chip systems in medicine, digital microfluidics has been used to extract DNA from whole blood samples,[28] quantify the levels of steroid hormones from breast tissue homogenates,[29] and screen for metabolic disorders and lysosomal storage diseases from newborn dried blood spots.[30–34] These examples highlight the fact that digital microfluidics is revolutionizing the field of portable medical diagnostics, and any rival technology needs to achieve the basic standards of droplet handling set by digital microfluidics.

In an attempt to emulate the droplet operations performed in digital microfluidics without the use of high electrical voltages or micromachining steps, we present a system where droplets are manipulated on a superhydrophobic surface (created on plastic sheets) by gravitational forces and mechanical agitation. The superhydrophobic plastic sheets are further printed with unique symbols using a hydrophilic ink. A microcontroller controls the direction and timing of two stepper motors which, in turn, provide mechanical agitation for droplet transport. Droplets remain confined to the hydrophilic symbols, and are able to 'hop' to neighbouring symbols by gravity when the surface is agitated and tilted to a certain degree. Using this basic principle, we illustrate the following droplet operations: transport of single and multiple droplets, transport of larger-volume droplets, merging and mixing of multiple droplets, dispensing of fixed-volume droplets from a large droplet or liquid reservoir, and one-directional movement of droplets. As a proof-of-concept, we show the application of the system as a colorimetric assay to detect the concentration of glucose in sheep serum.

Experimental

Design of the droplet actuation system

The motorized actuation system consists of a two-axis tilting platform to manipulate movement of discrete liquid droplets on hydrophilic symbols printed on a superhydrophobic surface. Fig. 1a shows the system configuration, including the three structural components: base, vertical column, and upper stage. The dimensions of these components are as follows: base (20 cm × 20 cm × 0.5 cm); vertical column (1 cm ×

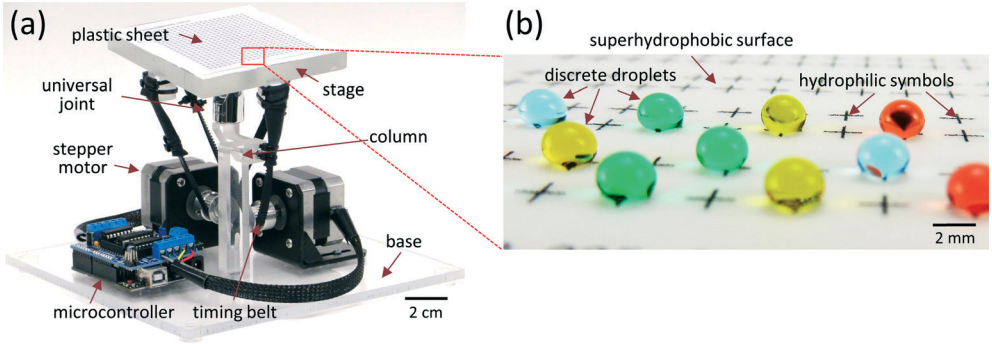

Fig. 1 The droplet actuation system. (a) The system comprises three structural components: base, column, and stage with plastic sheet. The base is physically screwed to the column. A universal joint connects the column to the stage. A microcontroller interfaces with two stepper motors (attached with individual timing belts) and controls the mechanical tilting of the stage. The plastic sheet is taped on the top of the stage. Scale bar = 2 cm. (b) A plastic sheet is spray-coated with a superhydrophobic chemical and printed with hydrophilic symbols using an inkjet printer. The image shows discrete droplets, each coloured with food dyes for visual illustration, resting on the hydrophilic symbols. Scale bar = 2 mm.

1 cm × 10 cm); upper stage (9 cm × 9 cm × 1.3 cm). The entire three-dimensional structure is designed in AutoCAD (Autodesk™) and the separate components are machined in acrylic glass (Plexiglas™). The stage is connected to the column by a universal joint that enables two-axis rotation about a central pivot. Two stepper motors (NEMA-17™, 200 steps per revolution, 12 volts, 350 milliamperes, bipolar mode) are connected with individual timing belts to the stage and mounted to the base. Each stepper motor controls one axis of rotation of the stage through an Arduino microcontroller (Adafruit Industries™). Single commands to tilt the stage up or down, left or right, and any sequence of such commands are programmed in a computer workstation and transmitted through a universal serial bus (USB) connection to the Arduino microcontroller. A graphical user interface (GUI) is designed for remote access to the droplet actuation system using a standard computer workstation (see ESI† Fig. S1). For image recording and characterization of droplet operations, a webcam (Logitech C920™) is positioned above the stage to monitor and record the simultaneous movement of multiple droplets.

Preparation of plastic sheets

After assembling the structural components of the droplet actuation system, we prepare the surface of plastic sheets that will serve as an open microfluidic arena to hold and move discrete droplets (Fig. 1b). Initially, letter-sized transparency films (Staples Inc.™) are rinsed with distilled water and spray-coated with a commercially available superhydrophobic coating (Rust-Oleum NeverWet™). The coating procedure is a two-step process that involves depositing a base coat and a top coat provided by the supplier. The base coat is applied by spraying on the surface of the transparency film. Three applications of the base coat are performed with a wait time of two minutes between successive applications. After drying for one hour, four applications of the top coat are performed in a similar fashion. The superhydrophobically-coated plastic sheet is dried for 12 hours at room temperature. Thereafter, hydrophilic symbols are printed on the plastic sheet by ink-jet printing. For this step, the plastic sheet is loaded into the document feeder of a commercial ink-jet printer (Epson WF-2540™). The layout of the desired symbols are drawn in Adobe Illustrator, saved on the computer, and printed using a black ink cartridge (Epson T200120™). After printing, the plastic sheet is dried for 12 hours at room temperature. Using the above procedure, a single letter-sized transparency film can produce six printed templates (9 cm × 9 cm) in one run.

Remote control and GUI software

A graphical user interface (GUI) software is developed in Matlab to remotely access and control the mechanical movement of the droplet actuation system. The Adafruit Motor Shield v1 communicates with the Arduino microcontroller through the I2C (Inter IC) protocol and controls each of the stepper motors. The Arduino is further controlled from a computer workstation using the Arduino Integrated Development Environment™. The GUI enables commands to be easily sent to the Arduino microcontroller. The script accepts inputs to set the speed and number of steps taken by the motors, which, in turn, controls the angular movement of the stage about the central pivot. The GUI has options to control motor parameters, such as the number of steps, speed of rotation, and direction of rotation which eventually control the angular movement of the stage about the central pivot. In the default state, the position of the stage is assumed horizontal and is calibrated using a bubble level (Camco Manufacturing Inc.™). When the GUI software is first run, the connection to the Arduino microcontroller is established automatically by searching active COM ports. Once the Arduino COM port is confirmed to be connected, the user can enter the sequence of mechanical operations to be performed. In the GUI window, pressing the double arrows increases the stage's angle of rotation in the corresponding direction (see ESI† Fig. S1). The single arrow button rapidly tilts the stage to a specified angle, and then returns it to the default horizontal position.

In addition, the GUI software communicates with a webcam to display a live preview of the top surface and record images or videos of droplet actuation.

Chemicals

Glucose assay kit (Sigma-Aldrich, GAGO20) is composed of the following chemicals: glucose oxidase/peroxidase (Sigma-Aldrich, G3660), and *o*-dianisidine reagent (Sigma-Aldrich, D2679). Glucose standard (Sigma-Aldrich, G6918) and sheep serum (Sigma-Aldrich, S3772) are also used. The glucose oxidase/peroxidase reagent is dissolved in 39.2 ml of deionized water. Next, *o*-dianisidine reagent is added in 1 mL of deionized water. The assay reagent is prepared by adding 0.8 mL of the *o*-dianisidine solution to the 39.2 mL of the glucose oxidase/peroxidase solution and mixing the solution thoroughly. The glucose standard solution is diluted to create 0.7 mg mL^{-1}, 0.6 mg mL^{-1}, 0.5 mg mL^{-1}, 0.4 mg mL^{-1}, 0.3 mg mL^{-1}, 0.2 mg mL^{-1}, and 0.1 mg mL^{-1} standards in deionized water. For control experiments, deionized water and black food dye (ACH Food Companies Inc.) are used.

Result and discussion

Transport of a single droplet

Fig. 2a shows the side-view of a single droplet placed on a hydrophilic symbol (left-side) printed on a superhydrophobic layer. As the stage is tilted clockwise, the droplet remains on the hydrophilic symbol. But, as the stage is quickly tilted anti-clockwise to the default horizontal position, the droplet slides down the superhydrophobic surface and rests on the neighbouring hydrophilic symbol (right-side). In Fig. 2b, side-view images of a single droplet are shown as it slides from the left symbol to the right one. The time for transporting a single 10 μL droplet between two consecutive symbols is approximately 100 milliseconds. The stage is tilted at 100 revolutions per minute (r.p.m.) and the number of steps is 14.

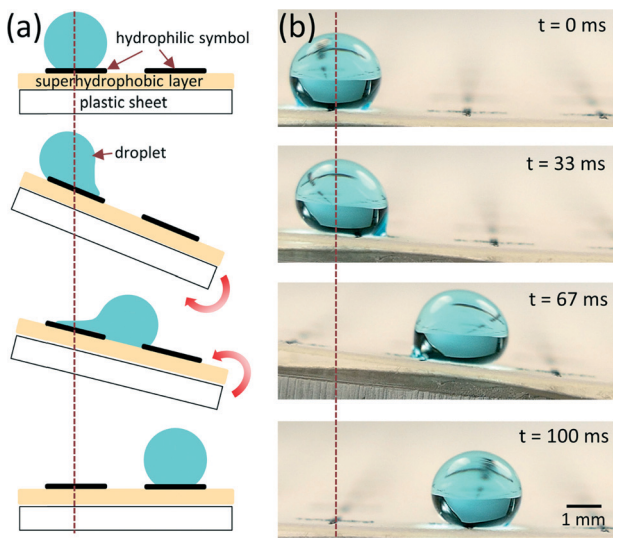

Fig. 2 Transport mechanism of a single droplet. (a) In the cartoon, a droplet is initially positioned on the left hydrophilic symbol printed on the superhydrophobic surface of a plastic sheet. The stage is tilted clockwise and then anti-clockwise to return to its default horizontal position (depicted by red block arrows). This rapid tilting action enables the droplet to move to the right hydrophilic symbol. (b) Time-lapsed images of an actual droplet show how the droplet is transported from the left symbol to the right symbol by the tilting action of the stage. The vertical dotted lines represents the starting position of the droplet. Scale bar = 1 mm.

The basic principle of droplet transport thus relies on positioning a droplet on a hydrophilic symbol and providing a rapid tilting action (*i.e.* tilting the stage clockwise (or anti-clockwise) to a specific angle followed by tilting the stage anti-clockwise (or clockwise) to the horizontal position). The rapid tilting action allows us to use small tilting angles (3–5°) with acceleration and deceleration of a droplet. Alternatively, a single droplet can be transported by slowly tilting the stage in one direction which, however, requires a larger tilting angle (9–20°) and provides no control on stopping the accelerated droplet.

We found that droplet transport can be controlled by a series of hydrophilic symbols printed at regular intervals. Based on initial tests, we chose to use 'plus (+)' symbols to demonstrate single droplet transport. Other symmetric symbols can also be used for this purpose. We printed plus symbols of different line widths and inter-symbol spacings (see ESI† Fig. S2a). The transport of single droplets on the different symbols is recorded, and an average displacement error is measured in each case. Negative displacement error occurs when a droplet fails to detach from the initial symbol. Conversely, positive displacement error occurs when the droplet travels beyond the neighbouring symbol (see ESI† Fig. S2c). In all cases, the droplet volume is 10 μL, tilting speed is 100 r.p.m., and number of steps is 14. The results indicate that symbols with thicker line widths produce negative displacement error as they have more surface area to hold the droplet in its original position (see ESI† Fig. S2b). On the other hand, symbols with thinner line widths produce positive displacement error as they have insufficient surface area to hold or capture a sliding droplet. The optimal line width is 0.02 cm and the inter-symbol spacing is 0.335 cm, which produces a negligible displacement error of 0.005 cm. We also found that, using this optimal dimension of the plus symbol, we can transport single droplets having a minimum and maximum water volume of 8 μL and 38 μL, respectively.

Physical model for droplet detachment from a hydrophilic symbol

Following the force balance analysis of Extrand and Gent,[35] we assume the contact region of a liquid droplet on the superhydrophobic surface is circular with a radius R. The droplet is about to detach from the hydrophilic symbol and travel downwards as the stage is tilted from its horizontal position to a critical angle α (see ESI† Fig. S3a). If the angular speed of the stage is ω revolutions per minute (r.p.m.) and the time for rotation is Δt minutes, then the critical angle α =

$2\pi\cdot\omega\cdot\Delta t$ radians. The parameterΔt can be further expressed as $\Delta t = N\cdot t_1$ minutes where N is the number of steps of the motor and t_1 is the time for one step rotation. The 'advancing edge' and 'receding edge' are labelled (see ESI† Fig. S3b). For the plus symbol, the hydrophilic line width is w and the length is $2 \times R$. The liquid droplet has a surface tension γ, contact angle θ, viscosity η, density ρ, volume V, radius r (such that $V = (4/3)\cdot\pi\cdot r^3$), and linear velocity v (such that $v = \omega\cdot\zeta$, where $\zeta = 3$ cm is the distance from the pivot to the center of stage). The azimuthal angle ϕ circumnavigates the perimeter of the contact region between a value of $\phi = 0$ at the rear end of the droplet to a value to $\phi = \pi/2$ at the advancing side of the droplet.

There are three forces acting on the droplet as the stage is tilted: surface tension F_{ST}, gravitation force F_G, and viscous force F_V. At the critical angle α of the stage, the individual forces balance as:

$$F_{ST} + F_V = F_G \tag{1}$$

In eqn (1), the surface tension force F_{ST} can be divided into two components: force F_r acting on the rear of the droplet and force F_a acting on the advancing front of the droplet. Plugging in the expressions for the gravitational force F_G acting parallel to the stage and the viscous force F_V, we get:

$$(F_r - F_a) + 6\cdot\pi\cdot\eta\cdot r\cdot v = \rho\cdot V\cdot g\cdot\sin\alpha \tag{2}$$

To compute the surface tension force, its component f per unit length of the contact perimeter varies along the perimeter as:[35]

$$f = \gamma\cdot\cos\theta\cdot\cos\phi \tag{3}$$

To simplify the calculation, we assume that $\cos\theta$ varies linearly around the perimeter of the contact region between a receding value of $\cos\theta_r$ at the rear end of the droplet (where $\phi = 0$) to an advancing value of $\cos\theta_a$ at the advancing side of the droplet (where $\phi = \pi/2$). For the case of a droplet on a homogeneous superhydrophobic surface, the expression for the contact angle is given by:[35]

$$\cos\theta = \frac{\phi}{\pi/2}\cdot\cos\theta_a + \left(1 - \frac{\phi}{\pi/2}\right)\cdot\cos\theta_r \tag{4}$$

Upon integration of eqn (3) and using eqn (4), the force acting on the rear of the drop F_r can be evaluated as:

$$F_r = 2\int_0^{\pi/2} f\cdot R\,\mathrm{d}\phi = 2\cdot R\cdot\gamma\int_0^{\pi/2}\cos\theta\cdot\cos\phi\,\mathrm{d}\phi \tag{5}$$

In our design with plus symbols, we modify eqn (4) to accommodate the role of hydrophilic symbol on the surface tension acting on the droplet (see ESI† Fig. S3b). In other words, the hydrophilic symbol produces an inhomogeneity in the surface tension which is accounted for by splitting the force contributions of the hydrophilic ink and the superhydrophobic surface.[36] We denote the advancing and receding contact angles on the hydrophilic ink as $\cos\theta_{a,ink}$ and $\cos\theta_{r,ink}$, respectively. Similarly, the advancing and receding contact angles on the superhydrophobic surface are denoted as $\cos\theta_{a,sub}$ and $\cos\theta_{r,sub}$, respectively. The parameter ϕ_1 indicates the azimuthal angle ϕ where the hydrophilic ink region changes to the superhydrophobic surface in the contact region, and is given by $\phi_1 = \sin^{-1}[w/(2\cdot R)]$.

Following from eqn (5), the force F_r acting on the rear of the droplet can be written as a sum of three forces:

$$F_r = 2\cdot R\cdot\gamma\left[\int_0^{\phi_1}\cos\theta_1\cdot\cos\phi\,\mathrm{d}\phi + \int_{\phi_1}^{\frac{\pi}{2}-\phi_1}\cos\theta_2\cdot\cos\phi\,\mathrm{d}\phi + \int_{\frac{\pi}{2}-\phi_1}^{\frac{\pi}{2}}\cos\theta_3\cdot\cos\phi\,\mathrm{d}\phi\right] \tag{6}$$

where

$$\cos\theta_1 = \frac{\phi}{\phi_1}\cdot\cos\theta_{r,sub} + \left(1 - \frac{\phi}{\phi_1}\right)\cdot\cos\theta_{r,ink} \tag{7}$$

$$\cos\theta_2 = \frac{\phi - \phi_1}{\frac{\pi}{2} - 2\phi_1}\cdot\cos\theta_{r,ink} + \frac{\frac{\pi}{2} - \phi_1 - \phi}{\frac{\pi}{2} - 2\phi_1}\cdot\cos\theta_{r,sub} \tag{8}$$

$$\cos\theta_3 = \frac{\phi - \frac{\pi}{2} + \phi_1}{\phi_1}\cdot\cos\theta_{a,ink} + \frac{\frac{\pi}{2} - \phi}{\phi_1}\cdot\cos\theta_{r,ink} \tag{9}$$

Similarly, the force F_a acting on the advancing front of the droplet can be written as a sum of three forces:[36]

$$F_a = 2\cdot R\cdot\gamma\left[\cos\theta_{a,ink}\int_0^{\phi_1}\cos\phi\,\mathrm{d}\phi + \cos\theta_{a,sub}\int_{\phi_1}^{\frac{\pi}{2}-\phi_1}\cos\phi\,\mathrm{d}\phi + \cos\theta_{a,ink}\int_{\frac{\pi}{2}-\phi_1}^{\frac{\pi}{2}}\cos\phi\,\mathrm{d}\phi\right] \tag{10}$$

Substituting eqn (6) and (10) into eqn (2), we can compute the critical angle α of the inclined stage where the gravitational force balances the surface tension and the viscous forces; thereby allowing the droplet to detach from the hydrophilic symbol and slide down the superhydrophobic surface.

To validate the physical model, experiments are conducted with water (density $\rho = 1$ g cm^{-3}, viscosity $\eta = 0.001$ Pa s, surface tension $\gamma_w = 72.8$ mN m^{-1}) and ethylene glycol (density $\rho = 1.11$ g cm^{-3}, viscosity $\eta = 0.0162$ Pa s, surface tension $\gamma_{EG} = 47.7$ mN m^{-1}) at temperature $T = 20$ °C. We measured the advancing and receding contact angles of the two liquids as: (a) water: $\theta_{a,ink} = 147°$, $\theta_{r,ink} = 81°$, $\theta_{a,sub} = 157°$, and $\theta_{r,sub} = 142°$

and (b) ethylene glycol: $\theta_{a,ink} = 134°$, $\theta_{r,ink} = 73°$, $\theta_{a,sub} = 140°$, and $\theta_{r,sub} = 126°$. The radius of the contact region is $R = 0.12$ mm. Table 1 shows the predicted and experimentally measured values of the critical angle α. The number of experiments (n) for each combination of line width and droplet volume is 10. In all cases, the predicted values lie within one standard deviation of the measured values.

It is worth noting that the viscosity of the liquid droplet is dependent on the concentration of dissolved electrolytes or sugars. The concentration-dependent viscosity of various sugar solutions can be modelled as:[37]

$$\eta = \eta_0 \cdot a \cdot \exp(E \cdot X) \quad (11)$$

where η_0 is the viscosity of pure water (in centiPoise) and X is the mole fraction in the solution. The parameters a and E are numerically estimated from experiments. In the case of glucose solutions, the values of the parameters are $a = 0.954$ and $E = 27.93$ for up to 60% maximum concentration at temperature $T = 20$ °C.[37]

Transport of multiple droplets and large-volume droplets

Using the abovementioned principle, the droplet actuation system can be used to transport multiple discrete droplets. As shown in Fig. 3, four droplets (each having 10 μL volume and coloured with different food dyes for visual illustration) are initially placed on separate plus symbols. For each symbol, the line width is 0.02 cm, line length is 0.24 cm, and inter-symbol spacing is 0.335 cm. The motor speed is 100 r.p.m. and the number of steps is 14. The red arrows in the figure indicate the direction of tilting the stage at each step. The stage is tilted to the right two times (Fig. 3a and b) and then downwards for three times (Fig. 3c–e). The final positions of the four droplets are shown in Fig. 3f. The images indicate that discrete droplets can be transported on a two-dimensional arrangement of plus symbols with virtually no risk of cross-contamination between droplets.

To address the challenge of transporting droplets having volumes greater than 38 μL, we designed arrays of plus symbols. Fig. 4a shows images of the 80 μL droplet being transported using a 2 × 2 array of plus symbols (line width is 0.0178 cm, line length is 0.24 cm, and inter-array spacing is 0.68 cm). Reducing the speed and increasing the number of steps of the motor (80 r.p.m., 20 steps) allows transport of the 80 μL droplet. Here, the stage is tilted once to the right (Fig. 4a-i and ii), once downwards (Fig. 4a-iii), and once to the left as depicted by the red arrows. The final position of the droplet is shown in Fig. 4a-iv. Using a similar approach, Fig. 4b shows images of the 300 μL droplet being moved using a 3 × 3 array of plus symbols (line width is 0.0178 cm, line length is 0.24 cm, and inter-array spacing is 0.94 cm). The motor speed is further reduced and the number of steps is increased to move this large droplet (60 r.p.m., 25 steps).

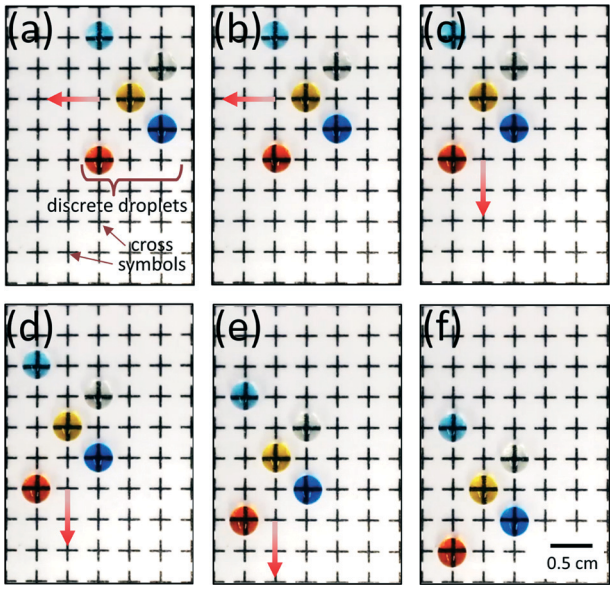

Fig. 3 Transport of multiple droplets: a series of images are taken to illustrate the movement of multiple droplets on an arrangement of plus symbols. The volume of each droplet is 10 μL and they are uniquely coloured with a food dye for visual illustration. The motor speed is 100 r.p.m. and the number of steps is 14. The direction of tilting the stage at every step is denoted by a red arrow. The stage is rapidly tilted twice in left direction (a, b) and three times in the downward direction (c–e). The final positions of all droplets are shown in (f). This demonstration shows that multiple droplets can be simultaneously moved in the same direction without any risk of cross-contamination. Scale bar = 0.5 cm.

Table 1 Critical sliding angle α of a droplet (water and ethylene glycol) is predicted from the physical model and compared from experiments on the actuation system. Three droplet volumes are tested (20 μL, 30 μL, and 40 μL); each droplet volume is tested on plus symbols having three different line widths (0.152 mm, 0.178 mm, and 0.203 mm). Every combination of droplet volume and line width is tested 10 times

Water				Ethylene glycol			
Droplet volume (μL)	Line width (mm)	Predicted α	Measured α	Droplet volume (μL)	Line width (mm)	Predicted α	Measured α
20	0.152	26.27°	24.1° ± 1.81°	20	0.152	20.99°	19.6° ± 1.36°
	0.178	26.40°	26.2° ± 1.94°		0.178	21.06°	20.9° ± 1.70°
	0.203	26.53°	28.5° ± 1.69°		0.203	21.13°	22.1° ± 1.42°
30	0.152	17.19°	15.7° ± 1.18°	30	0.152	14.32°	13.3° ± 0.93°
	0.178	17.28°	17.3° ± 1.62°		0.178	14.37°	14.8° ± 0.79°
	0.203	17.36°	18.2° ± 1.16°		0.203	14.41°	15.5° ± 0.81°
40	0.152	12.83°	11.7° ± 1.04°	40	0.152	10.99°	10.5° ± 0.81°
	0.178	12.89°	12.7° ± 1.34°		0.178	11.02°	10.9° ± 0.81°
	0.203	12.95°	13.4° ± 1.37°		0.203	11.05°	11.5° ± 0.72°

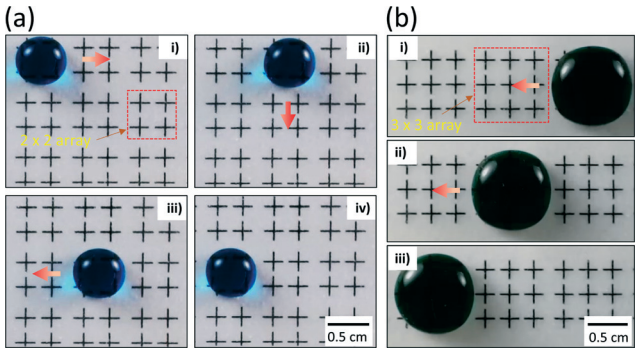

Fig. 4 Transport of large droplets: (a) a large blue droplet (volume = 80 μL) is moved using a 2 × 2 array of plus symbols (line width is 0.0178 cm, line length is 0.24 cm, and inter-array spacing is 0.68 cm). Compared to Fig. 3 where 10 μL droplets were moved, here the motor speed is decreased and the number of steps is increased (80 r.p.m., 20 steps) to move the 80 μL droplet. (b) A large green droplet (volume = 300 μL) is being transported to the neighbouring pattern using a 3 × 3 array of plus symbols. As in (a), the motor speed is decreased and the number of steps is increased (60 r.p.m., 25 steps) compared to those in Fig. 3. By using the same scheme and adjusting the parameters of stepper motors, up to 1 mL droplets have been transported. Scale bar = 0.5 cm.

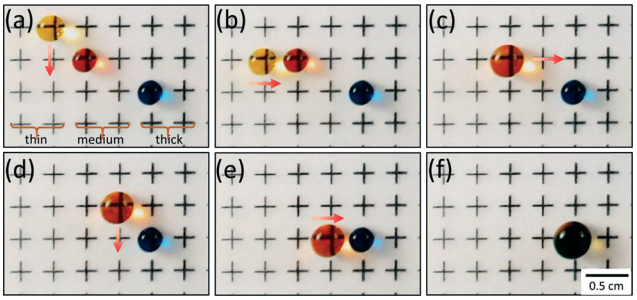

Fig. 5 Merging and mixing of multiple droplets. (a) A two-dimensional arrangement of plus symbols is shown where the line width is thinnest in the left two columns, medium thickness in the middle two columns, and thickest in the right two columns. Three droplets (yellow, red, and blue) are placed on the plus symbols. The red arrow indicates the direction of tilting the stage and the stage is tilted in the following sequence: downwards, right, right, downwards, and right. The yellow droplet is moved to and merged with the red droplet (a–c). This merged droplet is now moved and merged with the blue droplet (d–e) and the final product after merging all droplets is shown in (f). After the merging step, the stage can be agitated to mix the combined droplets. Scale bar = 0.5 cm.

Here, the stage is tilted to the left and the droplet settles on the neighbouring array of 3 × 3 symbols. Even though larger droplet volume can be transported by changing the design layout, we feel that the droplet volume of 300 μL adequately represents the maximum threshold needed for portable diagnostic testbeds.[29–33]

Merging and mixing of multiple droplets

The ability to bring two droplets together, merge and mix them, and repeat these steps sequentially with a finite number of discrete droplets is important for realizing on-chip chemical reactions. To achieve this ability, it is required that some droplets remain stationary while other droplets are being transported, merged or mixed together. This is accomplished by using plus symbols of different line widths, where symbols with thicker line widths have more holding force than symbols with thinner line widths. Fig. 5 shows images of a two-step merging and mixing performed on three droplets. The line widths of the plus symbols are thinnest in the left two columns (*i.e.* 0.015 cm holding the yellow droplet), medium thickness in the middle two columns (*i.e.* 0.02 cm holding the red droplet), and thickest in the right two columns (*i.e.* 0.025 cm holding the blue droplet). For all symbols, the line length is 0.24 cm and inter-symbol spacing is 0.37 cm. The intent here is to merge the yellow droplet with the red one, and subsequently merge their product with the blue droplet. The stage is tilted in the following sequence: downwards, right, right, downwards, and right (Fig. 5a–e). The red arrows indicate the direction of tilting the stage. The final product formed after merging all the three droplets is shown in Fig. 5f. It is interesting to note that the red and blue droplets are stationary when the yellow droplet is moved and merged with the red one (Fig. 5a and b), and the blue droplet is immobile throughout all the tilting operations. Thus, by adjusting the line widths of the plus symbols, we can selectively move one or more droplets to accomplish sequential merging operations. Post-merging, the mixing of two droplets is demonstrated in Fig. 5c and f by letting the merged product stay put on the symbol for some time (depending on the incubation time). This way of mixing by passive diffusion is satisfactory in case of droplets having soluble compounds. For droplets having immiscible or water-insoluble compounds, one can mix the droplets by agitating the stage (*i.e.* rapidly tilting the stage in alternate right and left directions in small angles) or moving the droplet in a circular pattern on neighbouring symbols.

One-directional transport of droplets

While the plus symbols allow us to move droplets in two dimensions (*i.e.* left and right, upwards and downwards) on the plastic sheet, there is also interest to control droplet transport in only one direction (*i.e.* left or right only, upwards or downwards only). Previously, this transport mechanism was demonstrated on a texture ratchet where vibrations at the resonance frequency produced directed motion of droplets.[15] To accomplish this task in our system, we used a 'greater-than (>)' symbol that allows us to move a droplet only to the right side (*i.e.* converging side of the symbol) upon tilting the stage in that direction. For each symbol, the line width is 0.023 cm and the length of each line is 0.33 cm. The acute angle between the two lines of the greater-than symbol is 28°. Fig. 6a shows images of two droplets; one placed on a greater-than symbol and the other on a plus symbol. The stage is tilted in the following sequence: right, left, right, and left. The droplet on the row of plus symbols follows the direction of stage tilting, and eventually returns to its original position. In comparison, the droplet on the

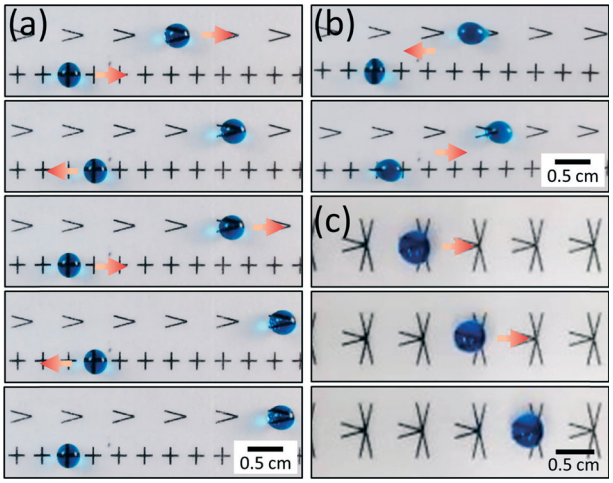

Fig. 6 (a) Each droplet is placed on two different symbols (plus and greater-than sign). The droplet on the plus symbol moves to the left when rapidly tilted to the left, but the droplet on the greater-than symbol does not move. When the substrate rapidly tilts to the right, both droplets on the plus symbol and the greater-than symbol move to the right. The acute point of the greater-than symbol has less hydrophilic area to attract the droplet. (b) Slow motion images showing different configurations of the droplet when the stage rapidly tilts to the left and right directions. When the stage tilts left, the two diagonal lines attached to the large area of the droplet prevent it from moving to next symbol. When the stage tilts right, a sharp point (where two diagonal lines meet) attaches to a small area of the droplet and the droplet is released to the next symbol. (c) One directional movement: the droplet only moves to the right due to the pattern of three converging greater-than symbols pointing to the center. Scale bar = 0.5 cm.

greater-than symbol is held at its original position when the stage is tilted to the left but moves to the right when the stage is tilted to the right. Fig. 6b shows the dynamics of the droplet on the greater-than symbol during the left or right tilting of the stage. During the left tilting, the droplet is still held in its original position due to the asymmetry of the greater-than symbol (on its left side compared to its right side). During the right tilting, the droplet volume concentrates to the narrow point of the symbol (on its right side) and is able to slide to the neighbouring symbol. Fig. 6c shows images of a droplet placed at the center of three converging greater-than symbols. Here the line width is 0.023 cm, length of each line is 0.33 cm, and the acute angle of each greater-symbol is 28°. Similar to Fig. 6a and b, this symbol also allows movement of droplets only to the right side but is able to hold the droplet on its central position even when the stage is tilted left, up or down. Thus one greater-than symbol prevents droplet movement in the left direction while the three converging greater-than symbols prevent droplet movement in the left, up, and down directions.

Dispensing smaller droplets from a large droplet

In wet chemistry experiments, it is often desired to pipette small volumes of reagents or samples repeatedly for multiple tests. As such, there is a need to generate equal volumes of smaller droplets from a large droplet (which may be a reagent or test sample). Typically, this is achieved in devices based on electrowetting[16–21] or by using a superhydrophobic blade to split a large droplet.[14] We accomplish this task by moving the large droplet over a series of circular dot symbols. Fig. 7a shows the side-view of a large red droplet moving over four dot symbols, and leaving behind a small droplet over each traversed symbol. Besides circular dot symbols, we can use rectangular or diamond-shaped symbols for dispensing small droplets, as shown in Fig. 7b and c, respectively (in all cases, the symbol area is 0.0097 cm^2). In Fig. 7d, we show how dispensing and mixing are performed sequentially. Here, a large red droplet moves over a row of dot symbols, leaving behind small droplets over each symbol (Fig. 7d-i–iii). Afterwards, a water droplet is moved over the same set of dot

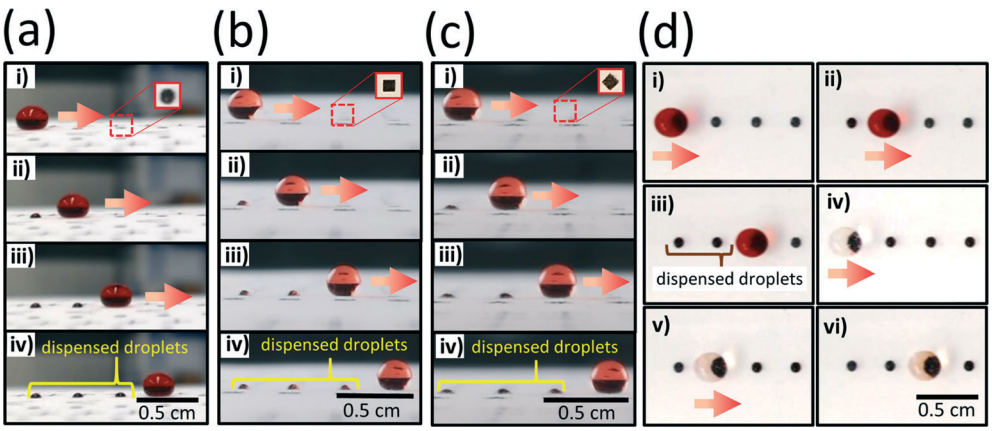

Fig. 7 Droplet dispensing from a large droplet (volume = 10 μL): (a) A small red droplet is dispensed on each circular dot hydrophilic symbol. While a large droplet moves over the hydrophilic dots, each symbol attracts the droplet and a small volume is left on each symbol. (b) Small red droplets are dispensed on rectangular-shaped hydrophilic symbols. (c) Small red droplets are dispensed on diamond-shaped hydrophilic symbol. (d) After the dispensing operation on circular dot symbols, a clear water droplet is transported across the dot symbols, causing the red colour intensity to increase in the clear droplet. Scale bar = 0.5 cm.

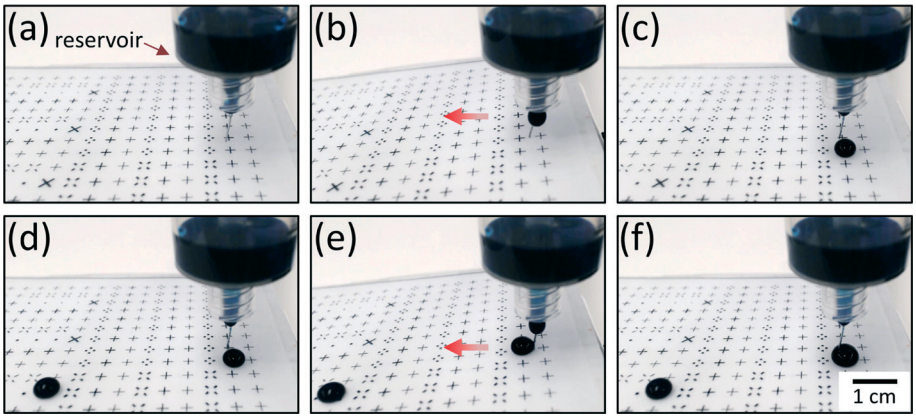

Fig. 8 Dispensing droplets from an external reservoir: (a) the reservoir is placed along the edge of the stage. (b) A dispenser tip is pressed by tilting the stage. (c) While the tip is pushed up, liquid flows out through the opened entrance of the reservoir. (d) A dispensed droplet is transported to another symbol and the next droplet is dispensed. (e, f) By tilting the stage twice, a larger droplet is dispensed in the same location. Scale bar = 1 cm.

symbols, thereby mixing the previously-left behind red droplets with water (Fig. 7d-iv–vi). We conducted experiments to measure the actual volume of small droplets left behind as a 10 μL water droplet travels over plus symbols and different-sized dot symbols (see ESI† Fig. S4, Tables S1 and S2). In addition to the fluid properties, the volume of droplets dispensed on the dot symbol is determined by the surface area of the symbol or surface defect,[38,39] which can be increased or decreased depending on the desired volume of dispensed droplets.

Dispensing droplets from an external reservoir

Besides dispensing smaller droplets from a large droplet, it is beneficial to develop a mechanism to dispense finite droplets from an external liquid reservoir that may contain a much larger liquid volume (*e.g.* cartridges, tubes, and syringes).[7] To achieve this method of dispensing, a syringe-based dispenser is realized. Here, the tip of a 20 mL syringe is cut, plugged by a 200 μL pipette tip, and then attached to a 1 mL syringe. The pipette tip is sealed with a cyanoacrylate adhesive along with a steel wire to extend the tip. This syringe-based dispenser is positioned above the plastic sheet on the stage (Fig. 8a). As the syringe tip faces downwards, gravitational force prevents liquid from back-flowing through the 20 mL syringe. When the stage is rapidly tilted, the steel wire is momentarily pushed up (Fig. 8b) to dispense a small droplet on the hydrophilic symbol underneath (Fig. 8c). This step can be repeated several times to dispense a series of discrete droplets from the reservoir (Fig. 8d–f).

Glucose detection

As a proof-of-concept, the droplet actuation system is employed to determine the glucose concentration in sheep serum using a colorimetric enzymatic test. The following reaction details the chemical reactions involved in the colorimetric test for glucose.[34]

$$\text{D-glucose} + H_2O + O_2 \xrightarrow{\text{glucose oxidase}} \text{D-gluconic acid} + H_2O_2 \quad (12)$$

$$H_2O_2 + \text{reduced } o\text{-dianisidine} \xrightarrow{\text{peroxidase}} \text{oxidized } o\text{-dianisidine} \quad (13)$$

In the presence of glucose oxidase, D-glucose is oxidized to D-gluconic acid and hydrogen peroxide. The colorless *o*-dianisidine reacts with hydrogen peroxide, in the presence of peroxidase, to form a brown-coloured oxidized *o*-dianisidine.

Initially, experiments are conducted in 24-well plates to characterize the colorimetric glucose assay. A standard glucose assay kit is used to prepare glucose solutions of different dilution factors. Around 250 μL of each solution is loaded into separate well plates, followed by 500 μL of assay reagent in each well. A webcam is used to record the colour of all well solutions for 30 minutes (frame rate: 29 frames per second). A Matlab script is written to extract the colour intensity of each well solution as a function of time. Specifically, the user selects different cropped areas in the first image. Then the script identifies the selected areas of all subsequent images in a video (see ESI† Fig. S8a). The 3-channel (RGB) images are converted into 1-channel (*i.e.* grayscale) images using ITU-R Recommendation BT.601, and the average colour intensity values are estimated as a function of time (see ESI† Fig. S8b). The colour intensity data are exported to a Microsoft Excel spreadsheet. The maximum slope for each solution (*i.e.* maximum change in colour intensity per second) is determined that correlates to the initial concentrations of glucose.[34] For each run with glucose samples, two control samples are used: deionized water with reagent and black food dye with reagent. The sheep serum is tested in a similar manner to give its glucose concentration (*i.e.* 0.59 mg mL^{-1}, see ESI† Fig. S8c), which is close to the value obtained from a microplate reader (*i.e.* 0.63 mg mL^{-1}).

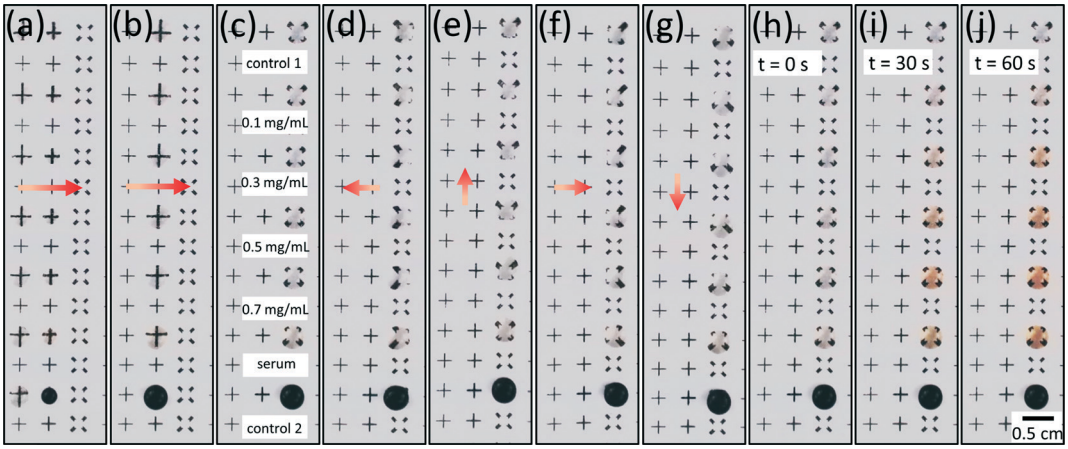

Fig. 9 Glucose detection on the droplet actuation system. (a) Glucose standards of different concentrations are placed on the middle column of plus symbols and the glucose reagents are placed on the leftmost column. (b) The stage is tilted to the right and the two columns of droplets merge on the middle column. (c) The merged droplets settle on the third column. (d–g) The stage is agitated in multiple directions to mix the combined droplets. (h–j) The merged droplets are incubated for the chemical reaction and the colour change is visible after around 10 seconds of incubation. The colour intensity is darker for droplets having higher glucose concentrations. Scale bar = 0.5 cm.

After conducting the well plate experiments, we performed a similar set of experiments on the droplet actuation system. After preparing the same dilutions of glucose solution, 5 μL droplets are placed on the middle column of plus symbols (line width = 0.015 cm) as shown in Fig. 9a. Another set of 10 μL glucose reagents are placed on the leftmost column of plus symbols (line width = 0.02 cm). When the stage is tilted to the right, the two columns of droplets (*i.e.* of glucose samples and reagents) merge on the middle column (Fig. 9b). Upon further tilting the stage to the right, the merged droplets settle on the rightmost column of X-shaped symbols (Fig. 9c) where they are agitated to be mixed thoroughly (Fig. 9d–g) and incubated for the chemical reaction (Fig. 9h–j). We found that agitating the stage reduces the mixing time of a merged droplet (using 5 μL red droplet and 20 μL yellow droplet) from 550 seconds with passive diffusion to 60 seconds with stage agitation (*i.e.* approximately a nine-fold reduction in mixing time) (see ESI† Fig. S5–S7). As shown in Fig. 9h, the colour change is visible after around 10 seconds of incubation. The higher the glucose concentration, the darker is the colour of the incubated droplet. The Matlab script accurately determines the average colour intensity of the droplets (Fig. 10a), which is later used to estimate the glucose concentrations in each droplet (Fig. 10b). The sheep serum is also tested in parallel with other glucose samples. Using the standard curve equation, the unknown glucose concentration of sheep serum is calculated as 0.62 mg mL^{-1}, which is close to the readings from the microplate reader and well plate experiments.

Table 2 summarizes the system parameters for the various droplet operations. Table 3 shows the flexibility of the system in transporting droplets having different fluid properties and different volumes. The three fluids tested are: water, milk, and ethylene glycol. Keeping the operating conditions fixed (*i.e.* motor speed = 100 r.p.m., number of steps = 14), we found that a wide range of droplet volumes (7 μL to 40 μL of water) can be transported on plus symbols (line width = 0.152 mm). However, under the same operating conditions, the range of droplet volumes transported on plus symbols decreases for a viscous liquid (12 μL to 26 μL of ethylene

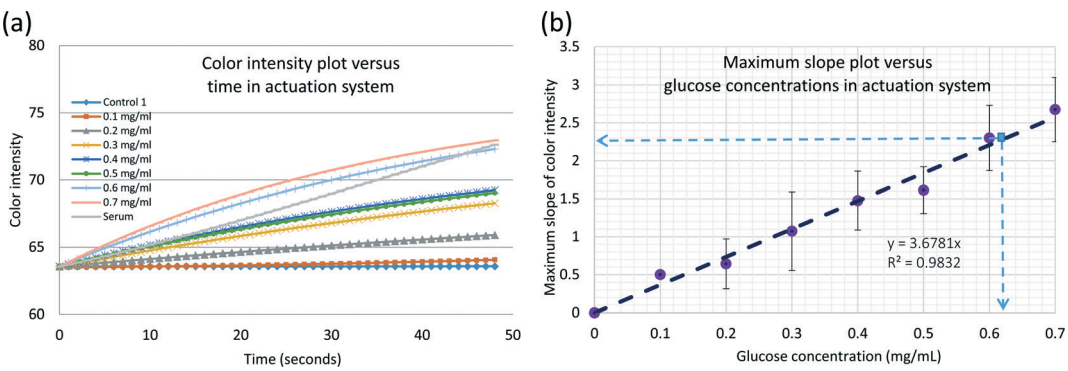

Fig. 10 Determination of glucose concentrations in sheep serum. (a) The colour intensities of incubated droplets at different time points are shown. Each glucose concentration is tested three times (n = 3). (b) The maximum slope of each colour intensity graph at different glucose concentrations is plotted to obtain the standard curve equation and to determine the glucose concentration in sheep serum.

Table 2 Values of the system parameters for the different droplet operations

Droplet operation	Figure number	Volume (μL)	Speed (r.p.m)	Steps N	Line width (cm)	Inter-symbol spacing (cm)
Single droplet transport	2	10	100	14	0.02	0.335
Multiple droplet transport	3	10	100	14	0.02	0.335
Large droplet transport	4(a)	80	80	20	0.0178	0.68
	4(b)	300	60	25	0.0178	0.94
Merging and mixing	5(a and b): left 2 columns	10	80	14	0.015	0.37
	5(c–e): middle 2 columns	20	90	14	0.02	0.37
	5(f): right 2 columns	30	0	0	0.025	0.37
One-directional transport	6(a and b)	10	100	14	0.023	0.37 (+)
	6(c)	20	100	14	0.023	0.74 (>)
						0.74
Dispending droplets	7(a–d)	10	100	14	Area = 0.0097 cm^2	0.37
Glucose detection	9(a): left column	10	100	14	0.015	0.45
	9(a): middle column	5	100	14	0.02	0.45
	9(c): rigth column	15	100	14	0.038	0.45
	9(d–g): rigth column	15	40	25	0.038	0.45
	9(i and j): rigth column	15	0	0	0.038	0.45

Table 3 The range of droplet volumes that can be transported on plus symbols is shown. Three different fluids are tested: water, milk, and ethylene glycol. The operating conditions of the motors is fixed (speed = 100 rpm, number of steps = 14). Each experiment on the minimum and maximum droplet volume is conducted 5–7 times

Fluid droplet	Fluid properties	Line width (mm)	Volume (μL)
Water	η = 0.001 Pa s	0.152	7–40
	ρ = 1 g cm^{-3}	0.203	8–38
	γ_w = 72.8 mN m^{-1}	0.254	10–36
Milk	η = 0.003 Pa s	0.152	7.5–38
	ρ = 1.032 g cm^{-1}	0.203	9–35
	γ_m = 52.4 mN m^{-1}	0.254	11–33
Ethylene glycol	η = 0.0162 Pa s	0.152	12–26
	ρ = 1.11 g cm^{-3}	0.203	17–24
	γ_{EG} = 47.7 mN m^{-1}	0.254	20–22

glycol). Supplemental videos show the real-time droplet operations performed on the droplet actuation system (see ESI† Videos S1–S3).

Conclusion

We demonstrated a droplet actuation system where discrete droplets are manipulated on hydrophilic patterns printed on a superhydrophobic plastic surface. Gravitational forces and mechanical agitation of the stage enable the transport of droplets. The system is designed for low-cost, resource limited settings where large area, disposable plastic sheets can be printed from standard inkjet printers and portable 9 V batteries power the motorized stage. We showed the possibility of transporting multiple droplets (volumes: 8 μL to 300 μL) in parallel and performing sequential fluidic reactions that will be beneficial to a variety of biological experiments. With the presented method, the design and layout of the hydrophilic symbols can be easily altered to specific functional requirements of an experiment. Lastly, the integration of smart image analysis tools with the droplet actuation system helps to automatically extract the parametric data, thereby minimizing human bias.

Acknowledgements

This work is partially supported by the U.S. National Science Foundation (NSF CBET-1150867 to S. P. and NSF DGE1247194 to R. B.). In addition, T. K. is partially supported by a grant from the Defence Threat Reduction Agency (HDTRA1-15-1-0053).

References

1 K. S. Elvira, X. C. Solvas, R. C. Wootton and A. J. deMello, *Nat. Chem.*, 2013, **5**, 905–915.
2 E. K. Sackmann, A. L. Fulton and D. J. Beebe, *Nature*, 2014, **507**, 181–189.
3 M. J. Jebrail, M. S. Bartsch and K. D. Patel, *Lab Chip*, 2012, **12**, 2452–2463.
4 M. G. Pollack, A. D. Shendorov and R. B. Fair, *Lab Chip*, 2002, **2**, 96–101.
5 K. Choi, A. H. C. Ng, R. Fobel and A. R. Wheeler, *Annu. Rev. Anal. Chem.*, 2012, **5**, 413–440.
6 W. C. Nelson and C.-J. Kim, *J. Adhes. Sci. Technol.*, 2012, **26**, 1747–1771.
7 A. Ghosh, R. Ganguly, T. M. Schutzius and C. M. Megaridis, *Lab Chip*, 2014, **14**, 1538–1550.
8 S. Y. Park, M. A. Teitell and E. P. Y. Chiou, *Lab Chip*, 2010, **10**, 1655–1661.
9 Z. Long, A. M. Shetty, M. J. Solomon and R. G. Larson, *Lab Chip*, 2009, **9**, 1567–1575.
10 J. Seo, S. Lee, J. Lee and T. Lee, *ACS Appl. Mater. Interfaces*, 2011, **3**, 4722–4729.
11 V. Jokinen, L. Sainiemi and S. Franssila, *Adv. Mater.*, 2008, **20**, 3453–3456.
12 Z. Wang and J. Zhe, *Lab Chip*, 2011, **11**, 1280–1285.
13 D. Foresti, M. Nabavi, M. Klingauf, A. Ferrari and D. Poulikakos, *Proc. Natl. Acad. Sci. U. S. A.*, 2013, **110**, 12494–12554.

14 H. Mertaniemi, V. Jokinen, L. Sainiemi, S. Franssila, A. Marmur, O. Ikkala and R. H. Ras, *Adv. Mater.*, 2011, **23**, 2911–2914.
15 T. A. Duncombe, E. Y. Erdem, A. Shastry, R. Baskaran and K. F. Bohringer, *Adv. Mater.*, 2012, **24**, 1545–1550.
16 J. Gong and C. J. Kim, *J. Microelectromech. Syst.*, 2008, **17**, 257–264.
17 C. Peng, Z. Zhang, C. J. Kim and Y. S. Ju, *Lab Chip*, 2014, **14**, 1117–1122.
18 S. C. Shih, P. C. Gach, J. Sustarich, B. A. Simmons, P. D. Adams, S. Singh and A. K. Singh, *Lab Chip*, 2015, **15**, 225–236.
19 S. Srigunapalan, I. A. Eydelnant, C. A. Simmons and A. R. Wheeler, *Lab Chip*, 2012, **12**, 369–375.
20 M. Abdelgawad, S. L. Freire, H. Yang and A. R. Wheeler, *Lab Chip*, 2008, **8**, 672–677.
21 C. J. Huang, W. F. Fang, M. S. Ke, H. Y. E. Chou and J. T. Yang, *Lab Chip*, 2014, **14**, 2057–2062.
22 B. Hadwen, G. R. Broder, D. Morganti, A. Jacobs, C. Brown, J. R. Hector, Y. Kubota and H. Morgan, *Lab Chip*, 2012, **12**, 3305–3313.
23 P. Y. Chiou, H. Moon, H. Toshiyoshi, C.-J. Kim and M. C. Wu, *Sens. Actuators, A*, 2003, **104**, 222–228.
24 R. Renaudot, V. Agache, Y. Fouillet, G. Laffite, E. Bisceglia, L. Jalabert, M. Kumemura, D. Collard and H. Fujita, *Lab Chip*, 2013, **13**, 4517–4524.
25 Z. Guttenberg, H. Müller, H. Habermüller, A. Geisbauer, J. Pipper, J. Felbel, M. Kielpinski, J. Scriba and A. Wixforth, *Lab Chip*, 2005, **5**, 308–317.
26 Z. Hua, J. L. Rouse, A. E. Eckhardt, V. Srinivasan, V. K. Pamula, W. A. Schell, J. L. Benton, T. G. Mitchell and M. G. Pollack, *Anal. Chem.*, 2010, **82**, 2310–2316.
27 H. Kim, M. S. Bartsch, R. F. Renzi, J. He, J. L. Van de Vreugde, M. R. Claudnic and K. D. Patel, *J. Lab. Autom.*, 2011, **16**, 405–414.
28 R. Sista, Z. Hua, P. Thwar, A. Sudarsan, V. Srinivasan, A. Eckhardt, M. Pollack and V. Pamula, *Lab Chip*, 2008, **8**, 2091–2104.
29 N. A. Mousa, M. J. Jebrail, H. Yang, M. Abdelgawad, P. Metalnikov, J. Chen, A. R. Wheeler and R. F. Casper, *Sci. Transl. Med.*, 2009, **1**, 1ra2.
30 C. Arnaud, *Chem. Eng. News*, 2011, **89**, 13–17.
31 R. S. Sista, A. E. Eckhardt, T. Wang, C. Graham, J. L. Rouse, S. M. Norton, V. Srinivasan, M. G. Pollack, A. A. Tolun, D. Bali, D. S. Millington and V. K. Pamula, *Clin. Chem.*, 2011, **57**, 1444–1451.
32 M. J. Jebrail, H. Yang, J. M. Mudrik, N. M. Lafreniere, C. McRoberts, O. Y. Al-Dirbashi, L. Fisher, P. Chakraborty and A. R. Wheeler, *Lab Chip*, 2011, **11**, 3218–3224.
33 S. C. C. Shih, H. Yang, M. J. Jebrail, R. Fobel, N. McIntosh, O. Y. Al-Dirbashi, P. Chakraborty and A. R. Wheeler, *Anal. Chem.*, 2012, **84**, 3731–3738.
34 V. Srinivasan, V. K. Pamula and R. B. Fair, *Anal. Chim. Acta*, 2004, **507**, 145–150.
35 C. Extrand and A. Gent, *J. Colloid Interface Sci.*, 1990, **138**, 431–442.
36 M. Elsharkawy, T. M. Schutzius and C. M. Megaridis, *Lab Chip*, 2014, **14**, 1168–1175.
37 J. Chirife and M. P. Buera, *J. Food Eng.*, 1997, **33**, 221–226.
38 J. Schneider, A. Egatz-Gomez, S. Melle, S. Lindsay, P. Dominguez-Garcia, M. A. Rubio, M. Marquez and A. A. Garcia, *Colloids Surf., A*, 2008, **323**, 19–27.
39 N. A. Patankar, *Langmuir*, 2003, **19**, 1249–1253.

